Lagrangian temperature and vertical velocity fluctuations due to gravity waves in the lower stratosphere

Aurélien Podglajen, Albert Hertzog, Riwal Plougonven, Bernard Legras

AGU PUBLICATIONS

Geophysical Research Letters

RESEARCH LETTER
10.1002/2016GL068148

Key Points:
- Long-duration balloon observations are used to characterize Lagrangian temperature fluctuations
- Intrinsic frequency spectra and PDFs are derived for temperature and cooling rates
- A parameterization of gravity wave temperature fluctuations in the lower stratosphere is developed

Supporting Information:
- Supporting Information S1

Correspondence to:
A. Podglajen,
apodgla@lmd.ens.fr

Citation:
Podglajen, A., A. Hertzog, R. Plougonven, and B. Legras (2016), Lagrangian temperature and vertical velocity fluctuations due to gravity waves in the lower stratosphere, *Geophys. Res. Lett.*, *43*, doi:10.1002/2016GL068148.

Received 5 FEB 2016
Accepted 18 MAR 2016
Accepted article online 22 MAR 2016

Lagrangian temperature and vertical velocity fluctuations due to gravity waves in the lower stratosphere

Aurélien Podglajen[1], Albert Hertzog[2], Riwal Plougonven[1], and Bernard Legras[1]

[1] Laboratoire de Météorologie Dynamique, CNRS-UMR8539, Institut Pierre Simon Laplace, École Normale Supérieure, École polytechnique, Université Pierre et Marie Curie, Paris, France, [2] Laboratoire de Météorologie Dynamique/IPSL, UPMC Univ Paris 06, CNRS, Palaiseau, France

Abstract Wave-induced Lagrangian fluctuations of temperature and vertical velocity in the lower stratosphere are quantified using measurements from superpressure balloons (SPBs). Observations recorded every minute along SPB flights allow the whole gravity wave spectrum to be described and provide unprecedented information on both the intrinsic frequency spectrum and the probability distribution function of wave fluctuations. The data set has been collected during two campaigns coordinated by the French Space Agency in 2010, involving 19 balloons over Antarctica and 3 in the deep tropics. In both regions, the vertical velocity distributions depart significantly from a Gaussian behavior. Knowledge on such wave fluctuations is essential for modeling microphysical processes along Lagrangian trajectories. We propose a new simple parameterization that reproduces both the non-Gaussian distribution of vertical velocities (or heating/cooling rates) and their observed intrinsic frequency spectrum.

1. Introduction

Microphysical processes in the tropical upper troposphere control the characteristics of ice clouds in the tropical tropopause layer (TTL) and the amount of water vapor that enters the stratosphere, which has significant implications on global climate, circulation response to climate change, and stratospheric ozone chemistry [*Solomon et al.*, 2010; *Randel and Jensen*, 2013; *Voigt and Shaw*, 2015]. At high latitudes, the formation of polar stratospheric clouds (PSCs) and the nature of nucleated particles is a crucial step in the chain of processes that contribute to ozone depletion [*Solomon et al.*, 1986]. In both cases, modeling of microphysical processes along air parcel trajectories computed with reanalyzed winds and temperatures has allowed estimations of key quantities, e.g., water vapor transport across the tropical tropopause and ozone loss [*Fueglistaler and Haynes*, 2005; *Grooß and Müller*, 2007; *James et al.*, 2008]. Yet several studies have highlighted that mesoscale wave motions, which are unresolved in the large-scale fields used for these simulations, actually have a strong influence on cloud characteristics, such as ice crystal number and particle size distribution for instance [see, e.g., *Murphy and Gary*, 1995; *Tabazadeh et al.*, 1996; *Haag and Kärcher*, 2004; *Hoyle et al.*, 2005; *Jensen et al.*, 2012; *Spichtinger and Krämer*, 2013; *Kärcher et al.*, 2014]. Microphysical processes indeed strongly depend on temperature, generally in a highly nonlinear way (with thresholds) so that relatively small temperature fluctuations may have a strong impact on particle nucleation [e.g., *Jensen et al.*, 2010; *Murphy*, 2014; *Dinh et al.*, 2016]. In Lagrangian microphysical simulations, it is therefore required to parameterize the unresolved small-scale high-frequency temperature and heating/cooling rate (or vertical velocity) fluctuations [*Bacmeister et al.*, 1999; *Jensen and Pfister*, 2004; *Haag and Kärcher*, 2004; *Jensen et al.*, 2012]. However, there are few observational constraints on these Lagrangian disturbances.

In fact, among meteorological variables, vertical velocities are certainly the least known. This is not only due to their small-scale structure, tied to gravity waves and convection, but also mainly due to a lack of observations. Only a few observing platforms are actually able to provide reliable estimates of vertical motions in the upper troposphere-lower stratosphere: Doppler lidar and radar [*Gage et al.*, 1986], inertial navigation systems on board scientific aircraft (e.g., Meteorological Measurement System) [*Muhlbauer et al.*, 2014] and superpressure balloons (SPBs). While vertical profiles of vertical velocity are inferred from remote-sensing measurements (lidar and radar), in situ platforms (aircrafts and balloons) generally provide local observations at higher space/time resolution. Among all the systems, superpressure balloons are unique because they are advected by the winds like air parcels. This quasi-Lagrangian behavior provides direct estimates of

wave-induced temperature and cooling/heating rate disturbances. Another attractive feature of SPBs is that as they are passively advected in the lower stratosphere, their sampling is a priori unbiased so that the collected data set is representative of day/night, land/ocean, and convective/clear sky conditions.

In this study, we take advantage of measurements performed during such SPB flights to describe the statistical and spectral properties of gravity wave disturbances in the lower stratosphere. Our main focus is to provide details on the vertical displacement and vertical velocity perturbations, which are respectively associated with temperature and heating/cooling rate fluctuations felt by air parcels in the atmosphere. The analyzed data set was collected during two SPB campaigns in 2010: the first one took place in the deep tropics in February–May and involved the flight of three superpressure balloons [*Podglajen et al.*, 2014], while 19 balloon flights were performed during the second campaign that took place over Antarctica and the Austral ocean in September 2010 to January 2011 [*Rabier et al.*, 2010].

The paper is organized as follows. In section 2, the balloon observations and their relationship to air parcel disturbances are introduced. Section 3 presents a spectral analysis of the time series, and section 4 describes the probability distributions of vertical wind disturbances and Lagrangian displacement inferred from the observations. Section 5 discusses different methods to parameterize wave-induced temperature and cooling rate fluctuations in Lagrangian models and describes a new one. The last section summarizes our findings.

2. Long-Duration Balloon Observations

2.1. Superpressure Balloon Campaigns

During the 2010 equatorial and polar campaigns, respectively named PreConcordiasi and Concordiasi, the French Space Agency (Centre National d'Etudes Spatiales, CNES) deployed closed, spherical, 12 m diameter SPBs. They drifted for durations close to 3 months on nearly constant density (∼0.1 kg/m^3) surfaces in the lower stratosphere, at about 19 km (PreConcordiasi) or 17 km (Concordiasi). Two of the three PreConcordiasi flights achieved circumterrestrial trajectories within 15° of the equator from February to May 2010 [*Podglajen et al.*, 2014], while the Concordiasi balloons flew from September to January and remained poleward of 60°S, within the decaying Southern Hemisphere stratospheric polar vortex.

The SPBs carried various instruments of interest for this study. All balloons were equipped with a GPS receiver, and the in situ horizontal winds were evaluated by finite differentiating the successive GPS positions, as in *Vial et al.* [2001]. In contrast to previous campaigns, positions were recorded every minute, giving access for the first time to the whole spectrum of gravity waves. The pressure measurements were performed every 30 s by the Thermodynamical SENsors meteorological package on board every balloon [*Hertzog et al.*, 2007]. Hence, as these measurements are performed in the frame of reference that moves with the wind (so-called intrinsic frame of reference), observations gathered during the 2010 SPB flights uniquely resolve the entire gravity wave spectrum, from the inertial (f) to the Brunt-Väisälä frequency (N). Regarding instrument performances, the estimated 1σ precisions of the GPS horizontal positions and pressure measurements, respectively, are 0.7 m and 0.1 Pa, and both measurement noises are assumed to behave as white noise processes.

2.2. Balloon Response to Air Motion

In order to correctly interpret the measured fluctuations, to understand their advantages and limitations, it is necessary to briefly discuss the response of the balloons to the surrounding air motions. Regarding horizontal motions, SPBs are advected by the horizontal wind, and their displacements therefore closely follow those of air parcels [*Massman*, 1978; *Vincent and Hertzog*, 2014]. Departures from the Lagrangian behavior in the horizontal are estimated to be within the uncertainty of GPS-derived winds [see, e.g., *Podglajen et al.*, 2014; *Vial et al.*, 2001].

The situation is different for the vertical motion of SPBs [e.g., *Massman*, 1978; *Nastrom*, 1980; *Vincent and Hertzog*, 2014]. While air parcels follow isentropes on timescales less than a few days in the lower stratosphere, superpressure balloons drift instead on isopycnic (constant density) surfaces as long as the wave-induced disturbances have intrinsic periods longer than twice the Brunt-Väisälä period ($2\pi/N$), i.e., longer than ∼10 min at the balloon flight level. In this "low-frequency" range, the balloon vertical displacement ζ'_b and that of an isentropic air parcel ζ'_θ are linearly related:

$$\zeta'_b = \alpha\zeta'_\theta \tag{1}$$

with α of the order of 0.3 [see, e.g., *Vincent and Hertzog*, 2014; *Podglajen et al.*, 2014] so that the vertical displacement and velocity of air parcels can be easily inferred from SPB motions. At higher frequencies

(i.e., gravity waves with intrinsic frequencies close to N and turbulence), the accuracy of this linear relationship becomes more questionable for two reasons: the main limitation results from the neutral oscillations of the balloons around their equilibrium level which happen at a frequency $\omega_b > N$ (the associated period, $2\pi/\omega_b$, is typically 3 min). The second cause for departures from isopycnic behavior is the inertia of the balloon, which needs to be taken into account for frequencies close to N [*Vincent and Hertzog*, 2014]. Finally, there is also a deviation from isopycnic behavior associated with the diurnal cycle in the balloon density, which is due to the slight expansion of the balloon envelope when heated by the Sun and has a typical peak-to-peak amplitude of 100–150 m.

3. Intrinsic Frequency Spectra of Atmospheric Motions

A unique characteristic of SPB measurements is that they directly record the intrinsic frequency ($\hat{\omega}$) of atmospheric disturbances, i.e., the frequency felt by air parcels, in contrast with ground-based instruments that measure frequencies affected by Doppler shift [see, e.g., *Vincent and Eckermann*, 1990; *Fritts and Wang*, 1991]. This is used below to obtain intrinsic frequency spectra of horizontal kinetic energy (E_{k_h}) and potential energy (E_p) and to quantify the contributions from low-frequency (planetary) and gravity waves. The spectra of temperature and vertical velocity fluctuations are then derived, as these are the relevant quantities for microphysical modeling.

3.1. Kinetic and Potential Energy Spectra

The wave potential and kinetic energy per unit mass, E_p and E_{k_h}, are

$$E_p = \frac{1}{2}N^2\zeta_\theta'^2, \qquad E_{k_h} = \frac{1}{2}(u'^2 + v'^2), \tag{2}$$

with ζ_θ' the (isentropic) wave-induced vertical displacement and u' and v' the wave-induced disturbances in zonal and meridional velocities.

In this study, $E_{k_h}(\hat{\omega})$ and $E_p(\hat{\omega})$ are obtained from independent sensors: E_{k_h} is directly deduced from the balloon horizontal velocities, whereas E_p is estimated from the balloon vertical displacements with the help of equation (1). In the latter equation, we use the high-precision pressure measurements to estimate the balloon vertical displacements; i.e., we assume that the variance in the measured pressure perturbations is essentially due to the Lagrangian component $\zeta_b'\mathrm{d}\overline{p}/\mathrm{d}z$ (where $\mathrm{d}\overline{p}/\mathrm{d}z$ is the vertical gradient of the background pressure). We thus neglect the variance induced by the Eulerian pressure perturbations, which is smaller than its Lagrangian counterpart by a factor of 3 at the very least (and generally a factor of 10) in the gravity wave frequency range.

Although estimated from independent measurements, these two spectra should nonetheless be closely linked if the observed disturbances are caused by gravity waves. Namely, using gravity wave polarization relations [e.g., *Fritts and Alexander*, 2003], one obtains

$$E_p = \left(\frac{N^2}{N^2 - \hat{\omega}^2}\right)\left(\frac{\hat{\omega}^2 - f^2}{\hat{\omega}^2 + f^2}\right)E_{k_h} \tag{3}$$

where f and $\hat{\omega}$ are, respectively, the inertial and wave intrinsic frequencies. This relation holds in the gravity wave frequency range ($f < \hat{\omega} < N$).

Figure 1 presents the one-dimensional intrinsic frequency spectra, for both the polar and equatorial campaigns. They were estimated as the average of several periodograms calculated from sequences of consecutive 8 day observations with 4 day overlaps. In the equatorial flights, balloon depressurizations (occurring when the balloons fly over cold, deep convective systems at night) were discarded because of the complex balloon response to air motion during these brief episodes.

3.1.1. Low-Frequency and Midfrequency Range

In the midfrequency regime (i.e., $f \ll \hat{\omega} \ll N$), the observed spectra of E_p and E_{k_h} have similar magnitudes within the uncertainty associated with spectral estimation. This is in agreement with equation (3) and confirms the gravity wave nature of the disturbances observed in that frequency range. Moreover, the spectra exhibit a robust power law behavior of gravity wave energy over a large range of frequencies and geographical locations. Yet the spectral slopes seem slightly different between the tropical and polar regions (see Table 1): the tropical spectra suggest a $\hat{\omega}^{-2}$ power law, whereas the polar flights exhibit a slightly shallower $\hat{\omega}^{-1.8}$ slope.

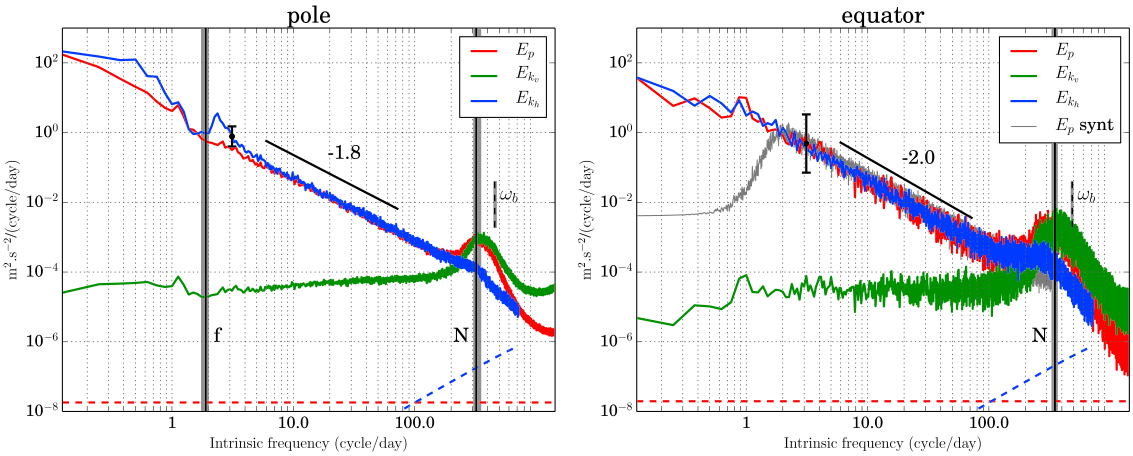

Figure 1. Spectra of potential (red), horizontal (blue), and vertical (green) kinetic energy, estimated from superpressure balloon observations collected during the 2010 (left) polar and (right) equatorial campaigns. On the right panel, the grey curve corresponds to the synthetic E_p signal described in section 5. The error bar indicates the confidence interval of the spectral estimates. The red and blue dashed lines correspond to the instrumental noise levels for potential and kinetic energy, respectively. The vertical black lines show the Coriolis frequency f for the polar flight and the Brünt-Väisälä frequency N (estimated from the European Centre for Medium-Range Weather Forecasts (ECMWF) operational analysis), the dashed line corresponds to the frequency of the balloon neutral oscillations ω_b (also estimated from the ECMWF operational analysis). The larger spectral uncertainty in the equatorial spectra is associated with a smaller number of flights during the PreConcordiasi campaign (3) than during the polar Concordiasi campaign (19).

It is known and expected that there is variability in spectral slopes, see for instance *Cho et al.* [1999a, 1999b] and *Dotzek and Gierens* [2008] for horizontal wave number wind and temperature spectra in the troposphere. Given the sampling available with our SPB measurements, the difference in slopes between the two regions appears statistically significant (see Table 1). However, at present, there is no theoretical argument to our knowledge that could attribute this difference to specific differences in wave sources or atmospheric structure between the polar and equatorial stratosphere.

Table 1. Major Characteristics of the Horizontal Kinetic Energy Spectra (Slope and 1σ Uncertainty), Lagrangian Temperature (or Vertical Displacements) and Vertical Velocity (or Heating/Cooling Rates) Disturbances Associated With Gravity Waves (GW) and Planetary Waves (PW) in the Superpressure Balloon Observations[a]

			Flights	
Spectral Characteristics	Motion	Frequency Range	Polar	Equatorial
E_{k_h} slope	GW	$2\pi/(4\,\mathrm{h})-2\pi/(20\ \mathrm{min})$	$-1.78(\pm0.01)$	$-1.96(\pm0.03)$
	GW	$2\pi/(12\ \mathrm{min})-2\pi/(6\ \mathrm{min})$	$-1.58(\pm0.02)$	$-0.48(\pm0.06)$
		$2\pi/(4\ \mathrm{min})-2\pi/(2\ \mathrm{min})$	$-3.36(\pm0.02)$	$-4.30(\pm0.03)$
$\sigma_{\zeta'}$ (m)/$\sigma_{T'_l}$ (K)	GW	f^b–N	66/0.64	110/1.07
	GW	$2f^c$–N	56/0.55	80/0.78
	PW	$2\pi/(20\,\mathrm{day})-2\pi/(1.5\,\mathrm{day})$	353/3.4	220/2.15
Kurtosis ζ'	GW	f^b–N	67	0.4
	GW	$2f^c$–N	112	0.8
$\sigma_{w'}$ ($\mathrm{m\,s^{-1}}$)/$\sigma_{\mathrm{D}T'_l/\mathrm{D}t}$ ($\mathrm{K\,h^{-1}}$)	GW	f^b–N	0.32/11.3	0.46/16.2
	GW	f^b–$N/2$	0.13/4.6	0.11/3.9
	PW	$2\pi/(20\,\mathrm{day})-2\pi/(1.5\,\mathrm{day})$	5×10^{-3}/0.18	3×10^{-3}/0.1
Kurtosis w'	GW	f^b–N	400	3.5
	GW	f^b–$N/2$	1310	5.8

[a]Normalized kurtosis values are all significantly different from 0, except the kurtosis of vertical displacements in equatorial flights.
[b]For the equatorial flights, we use a lower frequency bound of $2\pi/(1\ \mathrm{day})$.
[c]For the equatorial flights, we use a lower frequency bound of $2\pi/(12\ \mathrm{h})$.

At low frequencies, the polar E_{k_h} spectrum shows a distinct peak located close to the inertial frequency, which, in agreement with equation (3), has no equivalent in the potential energy spectrum. This low-frequency peak essentially remains an observational fact that has been already reported [e.g., *Hertzog et al.*, 2002]. The kinetic energy enhancement near f and the spectral gap between low-frequency planetary and inertia-gravity waves are striking characteristic of wave spectra at high latitudes. They are not seen in the equatorial spectra which, on the other hand, display a continuum of wave motions.

3.1.2. Higher-Frequency Range

At higher frequencies, the balloon observations suggest an interesting behavior near N with a local peak in potential energy, like a counterpart to the E_{k_h} peak at low frequencies in the polar flights. Caution is, however, needed in interpreting this peak, as the frequency of the balloon neutral oscillations ω_b is located close to N, and spurious (nonisopycnic) balloon vertical motions certainly contaminate the measurements at these high frequencies [*Vincent and Hertzog*, 2014].

We nevertheless argue in the supporting information that part of this high-frequency enhancement in E_p corresponds to real atmospheric motions. This rests on numerical simulations of SPB response to atmospheric motions, an alternative and independent determination of the E_p spectrum from the E_{k_h} one, and theoretical considerations on the expected evolution of vertical velocity disturbances along wave propagation. It is also worth noting that a similar peak near N has been previously reported in radar measurements in the troposphere, though with much smaller amplitudes [e.g., *Ecklund et al.*, 1985, 1986]. In any case, since the balloons overestimate the air parcel motions at frequencies close to N, further observations are needed to confirm the existence and assess the magnitude of this high-frequency peak in E_p.

On the other hand, a robust feature of E_p and E_{k_h} spectra is the sharp transition to much steeper slopes past N. In particular, the fact that the potential energy peak is located at N rather than at ω_b strongly supports the idea of weaker vertical motions at frequencies higher than N (cf. supporting information). This observed change of regime probably corresponds to the transition from gravity waves to isotropic turbulence. It is also noticed that this transition occurs at a slightly lower frequency than N on the equatorial E_{k_h} spectrum.

3.2. Vertical Velocity and Temperature Spectra

While considering energies emphasizes the agreement of balloon observations with gravity wave theory, the quantities that actually play a role in microphysical processes are the Lagrangian temperature disturbance and its temporal derivative along air parcel motions, the heating/cooling rate. The "Lagrangian" (adiabatic) temperature fluctuations are related to the wave-induced vertical displacement through

$$T_l' = -\frac{g}{C_p}\zeta_\theta' \tag{4}$$

in the dry adiabatic limit for a hydrostatic background atmosphere, where g and C_p are the gravity acceleration and the heat capacity of air at constant pressure, respectively. Hence, the spectrum of Lagrangian temperature disturbances follows

$$T_l'^2 = 2\left(\frac{g}{C_p N}\right)^2 E_p. \tag{5}$$

It is worth noting here that this Lagrangian temperature disturbance differs from the Eulerian value (T'), which is estimated at constant altitude. The Eulerian temperature disturbance is indeed related to E_p through

$$T'^2 = \bar{T}^2\left(\frac{\theta'}{\bar{\theta}}\right)^2 = 2\,\bar{T}^2\left(\frac{N}{g}\right)^2 E_p. \tag{6}$$

This "Eulerian" temperature variance is the one usually evaluated from radiosonde observations or constant altitude aircraft flights. Equations (5) and (6) show not only that both Eulerian and Lagrangian temperature spectra have similar $\hat{\omega}$ dependence as $E_p(\hat{\omega})$ but also that they differ by their magnitudes. In particular, for a given vertical displacement ζ_θ, the variance of Eulerian temperature disturbances depends on the background atmospheric stability, unlike the Lagrangian disturbances (see Text S3 in the supporting information for further details on this effect).

Besides temperature, microphysical processes such as ice nucleation also strongly depend on cooling rates and their intrinsic frequency distribution [e.g., *Kärcher and Lohmann*, 2002; *Dinh et al.*, 2016]. For adiabatic motions, those cooling rates are simply linked to the vertical velocity disturbance (w'):

$$\frac{\mathrm{D}T_I'}{\mathrm{D}t} = -\frac{g}{C_p}w', \tag{7}$$

whose spectrum is itself related to the E_p spectrum through

$$w'^2 = 2E_{k_v} = 2\left(\frac{\hat{\omega}}{N}\right)^2 E_p, \tag{8}$$

with $E_{k_v}(\hat{\omega})$, the vertical kinetic energy. On Figure 1, the E_{k_v} spectra are also displayed. They show a flat (or slightly increasing) variation with intrinsic frequency that highlights the importance of high-frequency waves in the variance of vertical velocity or heating/cooling rates. These spectra also display a strong peak at N. As previously discussed, the balloon measurements suggest that a fraction of this peak corresponds to real atmospheric motions but do not allow a quantitative assessment of this enhancement (see Text S1 in the supporting information).

4. Probability Density Functions (PDFs) and Intermittency

Beyond the frequency spectra that provide information on the temporal autocorrelation of temperatures and heating/cooling rates, it is also worth paying attention to the statistical distribution of these signals. Indeed, gravity wave activity is known to be intermittent [*Alexander et al.*, 2010; *Hertzog et al.*, 2012], and the sporadic character of wave disturbances can impact microphysical processes because of their strong nonlinearities.

4.1. Vertical Displacement (or Temperature) Statistics

As most of the variability in temperature (or vertical displacement) is contained in the low frequencies, we have applied a fifth-order high-pass Butterworth filter [e.g., *Oppenheim et al.*, 1999] to the temperature time series to isolate the gravity wave contribution from longer planetary wave signals. Figures 2a and 2b display the probability density function of temperature perturbations obtained with two different values for the cutoff frequency: f and $2f$ for the polar flights and 1 day^{-1} and 2 day^{-1} for the equatorial flights. The polar temperature PDF is essentially not sensitive to this choice because of the spectral gap between gravity and planetary waves, while the variance of the equatorial temperature disturbances depends more significantly on it (yet not the shape of the PDF).

The equatorial and polar PDFs exhibit very different shapes. The equatorial vertical displacement PDF suggests a Gaussian distribution (note the log y axis in Figure 2), with normalized kurtosis close to 0. The associated standard deviation is of the order of 100 m (1 K). On the contrary, the polar temperature PDF exhibits long tails and a much higher normalized kurtosis (67–112). If the standard deviations are smaller in the polar time series (66 m or 0.7 K), there is a more substantial contribution of unfrequent large displacements [*Bacmeister et al.*, 1999]. *Gierens et al.* [2007] also found non-Gaussian PDFs of temperature perturbations in data sets gathered during commercial aircraft flights, which mainly took place in the extratropical Northern Hemisphere upper troposphere. In a subsequent paper, *Dotzek and Gierens* [2008] attribute the emergence of those shapes to intermittency in temperature disturbances, which was at least partly caused by the aircraft crossing the tropopause. In our data set, the intermittency of gravity wave activity is the primary reason for the non-Gaussian behavior [*Hertzog et al.*, 2012]. A geographic screening furthermore shows that the long tails of the polar PDFs are associated with mountain waves over the Antarctic Peninsula (see Figure S3 in the supporting information).

In Table 1, the standard deviations of temperature fluctuations associated with both gravity and planetary waves signals are presented. The temperature PDFs and the reported variances show that the gravity wave contribution accounts for a significant fraction of the total wave perturbations and should therefore not be neglected when modeling microphysical processes. In the tropics for instance, gravity wave temperature fluctuations will, together with other wave motions, lower the mean cold-point tropopause temperature as well as its minima, which has impacts on dehydration in the TTL [*Kim and Alexander*, 2015].

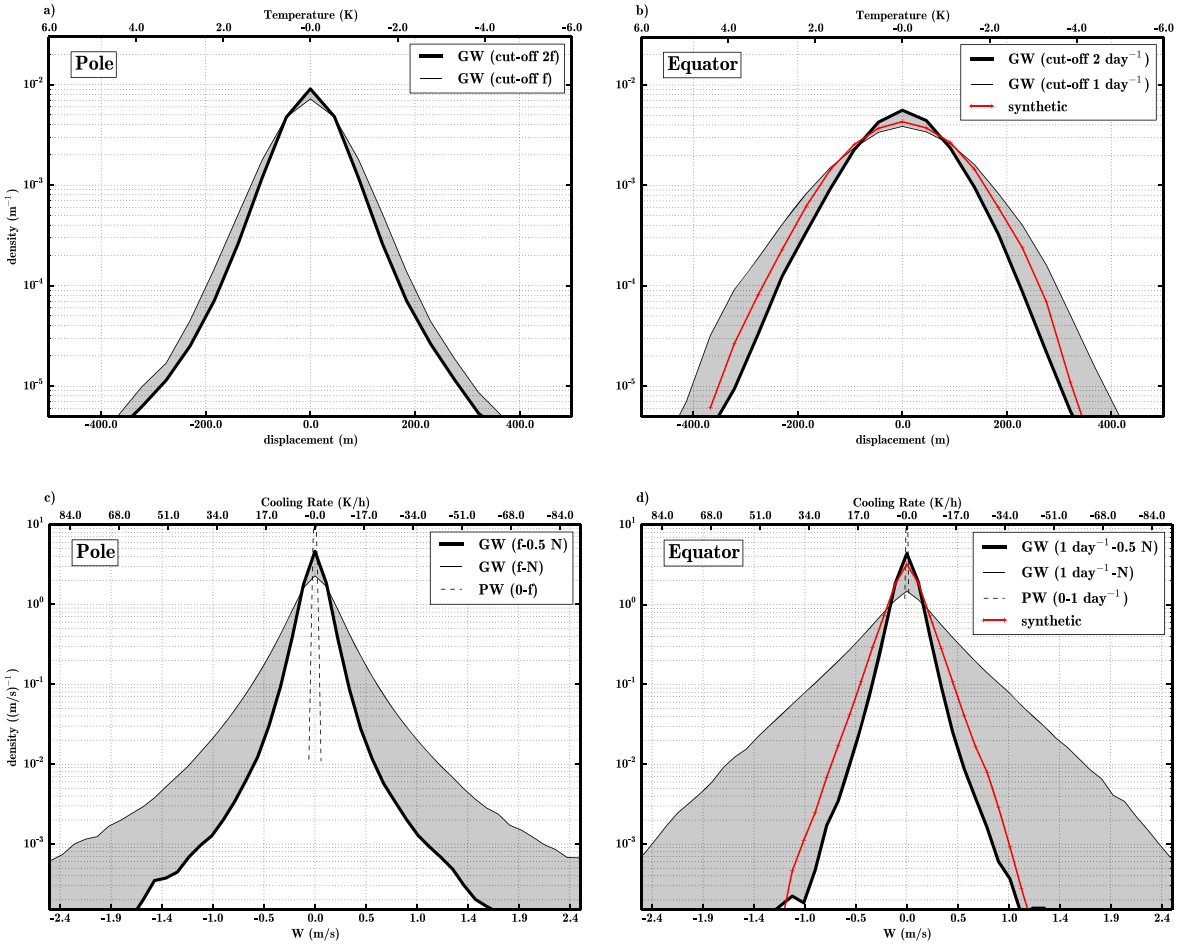

Figure 2. Probability density functions of (a, b) vertical displacements and (c, d) vertical velocities induced by gravity waves, for (Figures 2a and 2c) the polar and (Figures 2b and 2d) the equatorial balloon flights. For the vertical displacements (Figures 2a and 2b), two estimates that correspond to two different low cutoff frequencies (f and $2f$ in the polar flights, and 1 day^{-1} and 2 day^{-1} in the equatorial ones) are shown. The amplitude of the corresponding adiabatic temperature perturbations are shown on the upper x scale. For the (Figures 2c and 2d) vertical velocities, the two estimates correspond to two different high cutoff frequencies (N and $\frac{1}{2}N$) and the upper x scale shows the amplitude of the corresponding adiabatic cooling rates. The red curves in the Figures 2b and 2d correspond to the synthetic perturbations (see section 5).

4.2. Vertical Velocity (or Cooling Rates) Statistics

Unlike temperature fluctuations, most of the vertical velocity variance is associated with high-frequency motions. The frequencies of gravity waves extend to the Brunt-Väisälä frequency, but as previously mentioned the analysis of these high frequencies in the balloon measurements requires caution. In the following, we therefore show vertical velocity PDFs that have been obtained after applying a low-pass Kaiser filter [e.g., *Oppenheim et al.*, 1999] with cutoff frequencies located either at N or at $N/2$. The latter is a conservative choice (i.e., the spectral magnitude at this frequency is essentially void of any balloon-induced motions) that yields a lower bound for the total wave variance, since part of the full wave spectrum is omitted. The former, on the other hand, includes not only all wave motions but also some contributions associated with the balloon's own dynamics: it therefore corresponds to an upper bound of the wave variance.

The vertical velocity PDFs are displayed in Figures 2c and 2d for the two regions. In a more striking manner than for the vertical displacements, both tropical and high-latitude vertical velocity PDFs exhibit non-Gaussian shapes. The equatorial PDFs are close to a Laplace (double exponential) distribution. The polar PDFs even have distributions similar to double stretched exponentials. These shapes underline the important intermittency in the vertical velocity field, i.e., that the largest cooling rates are significantly more frequent than in a Gaussian distribution. They are likely to influence microphysical processes in the upper troposphere or lower stratosphere. For instance, the large tails that are primarily associated with mountain waves have a substantial impact on wave-driven PSC formation [e.g., *Carslaw et al.*, 1999].

We also show on Figures 2c and 2d the vertical velocity PDF associated with planetary waves, which are obtained by keeping only motions with intrinsic frequencies smaller than f (or 1 day^{-1}) in the balloon time series. Figure 2 highlights that the contribution of these low-frequency motions to the vertical velocities or cooling rates is very small, consistently with the slope of the corresponding spectrum. Almost all of the vertical velocity perturbations are due to gravity waves in the tropics and high latitudes, which once again supports the need to parameterize gravity wave fluctuations when modeling microphysical processes.

5. Parameterizations of Gravity Wave Fluctuations in Lagrangian Models

Lagrangian trajectory models targeting cloud or aerosol processes generally use large-scale analysis fields that are archived every few hours. In those models, different strategies have been used to represent shorter gravity wave temperature fluctuations and to reproduce either their spectra or their PDFs. In section 5.2, a new parameterization is proposed, which allows to reproduce both.

5.1. Existing Parameterizations

Aiming at simulating polar stratospheric clouds formation, *Bacmeister et al.* [1999] introduced a parameterization that consists in a discrete sum of harmonics with different frequencies, where the phase of each harmonic is attributed randomly while the amplitude is chosen to match prescribed spectral magnitudes. *Jensen and Pfister* [2004] used a similar approach for TTL cirrus clouds and constrained the harmonic amplitudes with measurements from long-duration balloon flights reported in *Hertzog and Vial* [2001]. This type of parameterization reproduces the observed slopes and magnitudes of the temperature and cooling rate spectra, but the use of random phases generates Gaussian PDFs. Such PDFs differ from observed cooling rate PDF in the tropics and from both temperature and cooling rate PDFs at high latitude.

Other methods to synthesize wave-induced fluctuations have included white noise [*Gary*, 2006] or multifractal random noise [*Murphy*, 2014] . If the use of white noise for temperature fluctuations easily allows the simulation of any PDF, it is in obvious contrast with the robust red spectra seen in the balloon observations. In fact, a white noise for cooling rate disturbances would be in closer agreement with the observations. *Murphy* [2003] and *Murphy* [2014] used multifractal random noise (using multiplicative cascades), for which one can control the spectral slope but did not provide any details on the temperature or cooling rate fluctuations PDFs.

Another approach for specific case studies is the use of a high-resolution nonhydrostatic model with output at high frequency, which can serve to compute trajectories resolving fast temperature fluctuations [*Kienast-Sjögren et al.*, 2015].

5.2. A New Parameterization for Temperature and Vertical Velocity Fluctuations

Based on the balloon observations, we propose an alternative way to parameterize wave-induced fluctuations by using a stochastic model. The synthetic time series generated by this parameterization agree with the balloon observations in the sense that they reproduce both the spectral shapes and the non-Gaussian cooling rate PDF. The tropical case is an especially favorable case, because the observed spectrum of temperature disturbances scales as $\hat{\omega}^{-2}$ and the associated PDF is nearly Gaussian. In this case, an autoregressive model of order 1, or Markov process, is sufficient to synthesize time series that resemble the observations. The displacement field ζ' is thus generated iteratively:

$$\zeta'_{t+dt} = \zeta'_t + W \cdot \mathrm{d}t\,, \tag{9}$$

where W is a white noise process that corresponds to the vertical velocity and follows a Laplace (double exponential) distribution. A 2 day^{-1} high-pass Butterworth filter is applied on the raw time series in order to remove its low-frequency component that should be resolved in the large-scale analysis. To match the balloon observations, the value of the free parameters are dt=2.2 min and the standard deviation of the Laplace white noise is 0.17 m/s. The Butterworth high-pass filter is of fifth order, and further details on the method are provided in the supplementary materials.

Figure 1 shows that the synthetized time series matches the slope and magnitude of the potential and kinetic energy spectra in the midfrequency range, up to $\frac{N}{2}$. Figures 2b and 2d illustrate that the PDFs of both temperature and vertical velocity can be reproduced. It should be noted that we take advantage of the flat vertical velocity spectrum, which easily allows us to match the observed cooling rate PDF. On the other hand, the Gaussian shape of the resulting temperature PDF results from the central limit theorem, and more sophisticated techniques would be needed to reproduce a non-Gaussian shape, as is observed over the pole (Figure 2).

Since the tails of this polar temperature PDF are tied to mountain waves over specific regions (e.g., the Antarctic Peninsula), we agree with the suggestion of *Bacmeister et al.* [1999] that a dedicated parameterization of intermittent, intense orographic events is additionally required, as for instance done in *Carslaw et al.* [1999]. When the balloon data set is considered only over oceanic regions around Antarctica, the PDF of temperature fluctuations becomes more Gaussian, and our method succeeds in producing synthetic time series that mimic this perturbation background (see supporting information).

In the above example, the free parameters have been chosen to match SPB observations in the lower stratosphere. They would need to be adjusted to mimic temperature and vertical velocity fluctuations at a different time period (e.g., polar winter instead of spring) or at a different height (e.g., a few kilometers lower in the TTL). Such adjustment is described in the supporting information. Alternatively, the parameters may also be adjusted to reproduce the vertical velocity or Eulerian temperature statistics obtained from non-Lagrangian observations.

6. Summary

This letter has presented measurements of Lagrangian temperature and vertical velocity fluctuations in the tropical and polar lower stratosphere. The specificity of superpressure balloons and the high temporal resolution of the measurements gives an unprecedented opportunity to describe Lagrangian fluctuations tied to the entire wave spectrum, including gravity waves up to the Brunt-Väisälä frequency. The measurements were collected over specific regions during $\sim$ 3 month time periods: southern high latitudes during austral spring and deep tropics during boreal spring and easterly shear phase of the quasi-biennal oscillation. We note that seasonal variations of wave activity are expected to be important at high latitudes [e.g., *Geller et al.*, 2013]. In the tropics, on the other hand, the representativeness of the SPB data set is probably better because of the sampling of both clear skies and convection during the flights.

Our results confirm the $\hat{\omega}^{-2}$ power law behavior of potential and kinetic energy spectra in the midfrequency range ($f \ll \hat{\omega} \ll N$) for both the tropical and polar regions. Yet the observations also suggest a local enhancement of wave energy when N is approached, which may result from geophysical processes such as wave refraction and reflection or high-frequency wave sources (e.g., convection). Unfortunately, the amplitude of this local maximum near N cannot be assessed with current balloon observations because of the nonlinear response of SPBs to atmospheric motions with very high frequencies. On the other hand, the wave vertical velocity spectrum is essentially flat for $\hat{\omega} < N/2$, which is a direct consequence of the potential energy spectral slope and gravity wave polarization relations. Hence, high-frequency perturbations provide the major contribution to the whole wave vertical velocity variability.

Generally, the probability distributions of vertical velocity and temperature disturbances are not Gaussian, because of gravity wave intermittency. This is especially true in the polar flights that are affected by highly intermittent orographic sources, like over the Antarctic peninsula [*Hertzog et al.*, 2008]. In the tropical flights, the temperature perturbations are normally distributed but not the vertical velocity disturbances, which rather follow a Laplace distribution.

We propose a new parameterization of wave-induced temperature and heating/cooling rates in Lagrangian models. Crucially, this parameterization reproduces both the observed wave spectra and PDFs. Its simplicity makes it straightforward to implement in studies along air parcel trajectories, which address processes that depend on wave-induced fluctuations.

Acknowledgments

SPB data used in this study can be obtained upon request from A.H. (albert.hertzog@lmd.polytechnique.fr). Concordiasi is an international project, currently supported by the following agencies: Météo-France, CNES, CNRS/INSU, NSF, NCAR, University of Wyoming, Purdue University, University of Colorado, the Alfred Wegener Institute, the Met Office, and ECMWF. Concordiasi also benefits from logistic or financial support of the operational polar agencies (Institut Polaire Franais Paul Emile Victor) IPEV, Programma Nazionale di Ricerche in Antartide (PNRA), United States Antarctic Program (USAP) and (British Antarctic Survey) BAS, and from Baseline Surface Radiation Network (BSRN) measurements at Concordia. Concordiasi is part of The Observing System Research and Predictability Experiment International Polar Year (THORPEX-IPY) cluster within the International Polar Year effort. The authors acknowledge support from the StraDyVariUS project (ANR-13-BS06-0011-01) funded by ANR.

References

Alexander, M. J., et al. (2010), Recent developments in gravity-wave effects in climate models and the global distribution of gravity-wave momentum flux from observations and models, *Q. J. R. Meteorol. Soc.*, *136*(650), 1103–1124, doi:10.1002/qj.637.

Bacmeister, J. T., S. D. Eckermann, A. Tsias, K. S. Carslaw, and T. Peter (1999), Mesoscale temperature fluctuations induced by a spectrum of gravity waves: A comparison of parameterizations and their impact on stratospheric microphysics, *J. Atmos. Sci.*, *56*, 1913–1924, doi:10.1175/1520-0469.

Carslaw, K. S., T. Peter, J. T. Bacmeister, and S. D. Eckermann (1999), Widespread solid particle formation by mountain waves in the Arctic stratosphere, *J. Geophys. Res.*, *104*(D1), 1827–1836, doi:10.1029/1998JD100033.

Cho, J. Y. N., Y. Zhu, R. E. Newell, B. E. Anderson, J. D. Barrick, G. L. Gregory, G. W. Sachse, M. A. Carroll, and G. M. Albercook (1999a), Horizontal wavenumber spectra of winds, temperature, and trace gases during the Pacific Exploratory Missions: 1. Climatology, *J. Geophys. Res.*, *104*(D5), 5697–5716, doi:10.1029/98JD01825.

Cho, J. Y. N., R. E. Newell, and J. D. Barrick (1999b), Horizontal wavenumber spectra of winds, temperature, and trace gases during the Pacific Exploratory Missions: 2. Gravity waves, quasi-two-dimensional turbulence, and vortical modes, *J. Geophys. Res.*, *104*(D13), 16,297–16,308, doi:10.1029/1999JD900068.

Dinh, T., A. Podglajen, A. Hertzog, B. Legras, and R. Plougonven (2016), Effect of gravity wave temperature fluctuations on homogeneous ice nucleation in the tropical tropopause layer, *Atmos. Chem. Phys.*, *16*, 35–46, doi:10.5194/acp-16-35-2016.

Dotzek, N., and K. Gierens (2008), Instantaneous fluctuations of temperature and moisture in the upper troposphere and tropopause region. Part 2: Structure functions and intermittency, *Meteorol. Z.*, *17*(3), 323–337, doi:10.1127/0941-2948/2008/0292.

Ecklund, W. L., B. B. Balsley, D. A. Carter, A. C. Riddle, M. Crochet, and R. Garello (1985), Observations of vertical motions in the troposphere and lower stratosphere using three closely spaced ST radars, *Radio Sci.*, *20*(6), 1196–1206, doi:10.1029/RS020i006p01196.

Ecklund, W. L., K. S. Gage, G. D. Nastrom, and B. B. Balsley (1986), A preliminary climatology of the spectrum of vertical velocity observed by clear-air Doppler radar, *J. Clim. Appl. Meteorol.*, *25*(7), 885–892, doi:10.1175/1520-0450(1986)025<0885:APCOTS>2.0.CO;2.

Fritts, D. C., and M. J. Alexander (2003), Gravity wave dynamics and effects in the middle atmosphere, *Rev. Geophys.*, *41*(1), 1003, doi:10.1029/2001RG000106.

Fritts, D. C., and D.-Y. Wang (1991), Doppler-shifting effects on frequency spectra of gravity waves observed near the summer mesopause at high latitude, *J. Atmos. Sci.*, *48*(13), 1535–1544, doi:10.1175/1520-0469(1991)048<1535:DSEOFS>2.0.CO;2.

Fueglistaler, S., and P. H. Haynes (2005), Control of interannual and longer-term variability of stratospheric water vapor, *J. Geophys. Res.*, *110*, D24108, doi:10.1029/2005JD006019.

Gage, K. S., B. B. Balsley, and R. Garello (1986), Comparisons of horizontal and vertical velocity spectra in the mesosphere, stratosphere and troposphere: Observations and theory, *Geophys. Res. Lett.*, *13*(11), 1125–1128, doi:10.1029/GL013i011p01125.

Gary, B. L. (2006), Mesoscale temperature fluctuations in the stratosphere, *Atmos. Chem. Phys.*, *6*(12), 4577–4589, doi:10.5194/acp-6-4577-2006.

Geller, M. A., et al. (2013), A comparison between gravity wave momentum fluxes in observations and climate models, *J. Clim.*, *26*(17), 6383–6405, doi:10.1175/JCLI-D-12-00545.1.

Gierens, K., R. Kohlhepp, N. Dotzek, and H. G. Smit (2007), Instantaneous fluctuations of temperature and moisture in the upper troposphere and tropopause region. Part 1: Probability densities and their variability, *Meteorol. Z.*, *16*(2), 221–231, doi:10.1127/0941-2948/2007/0197.

Grooß, J.-U., and R. Müller (2007), Simulation of ozone loss in Arctic winter 2004/2005, *Geophys. Res. Lett.*, *34*, L05804, doi:10.1029/2006GL028901.

Haag, W., and B. Kärcher (2004), The impact of aerosols and gravity waves on cirrus clouds at midlatitudes, *J. Geophys. Res.*, *109*, D12202, doi:10.1029/2004JD004579.

Hertzog, A., and F. Vial (2001), A study of the dynamics of the equatorial lower stratosphere by use of ultra-long-duration balloons: 2. Gravity waves, *J. Geophys. Res.*, *106*(D19), 22,745–22,761, doi:10.1029/2000JD000242.

Hertzog, A., F. Vial, C. R. Mechoso, C. Basdevant, and P. Cocquerez (2002), Quasi-lagrangian measurements in the lower stratosphere reveal an energy peak associated with near-inertial waves, *Geophys. Res. Lett.*, *29*(8), 1229, doi:10.1029/2001GL014083.

Hertzog, A., et al. (2007), Stratéole/vorcore—Long-duration, superpressure balloons to study the Antarctic lower stratosphere during the 2005 winter, *J. Atmos. Oceanic Technol.*, *104*(D1), 2048–2061, doi:10.1175/2007JTECHA948.1.

Hertzog, A., G. Boccara, R. A. Vincent, F. Vial, and P. Cocquerez (2008), Estimation of gravity wave momentum flux and phase speeds from quasi-Lagrangian stratospheric balloon flights. Part II: Results from the Vorcore campaign in Antarctica, *J. Atmos. Sci.*, *65*(10), 3056–3070, doi:10.1175/2008JAS2710.1.

Hertzog, A., M. J. Alexander, and R. Plougonven (2012), On the intermittency of gravity wave momentum flux in the stratosphere, *J. Atmos. Sci.*, *69*(11), 3433–3448, doi:10.1175/JAS-D-12-09.1.

Hoyle, C. R., B. P. Luo, and T. Peter (2005), The origin of high ice crystal number densities in cirrus clouds, *J. Atmos. Sci.*, *62*, 2568–2579, doi:10.1175/JAS3487.1.

James, R., M. Bonazzola, B. Legras, K. Surbled, and S. Fueglistaler (2008), Water vapor transport and dehydration above convective outflow during Asian monsoon, *Geophys. Res. Lett.*, *35*, L20810, doi:10.1029/2008GL035441.

Jensen, E., and L. Pfister (2004), Transport and freeze-drying in the tropical tropopause layer, *J. Geophys. Res.*, *109*, D02207, doi:10.1029/2003JD004022.

Jensen, E. J., L. Pfister, T.-P. Bui, P. Lawson, and D. Baumgardner (2010), Ice nucleation and cloud microphysical properties in tropical tropopause layer cirrus, *Atmos. Chem. Phys.*, *10*(3), 1369–1384, doi:10.5194/acp-10-1369-2010.

Jensen, E. J., L. Pfister, and T. P. Bui (2012), Physical processes controlling ice concentrations in cold cirrus near the tropical tropopause, *J. Geophys. Res.*, *117*, D11205, doi:10.1029/2011JD017319.

Kärcher, B., and U. Lohmann (2002), A parameterization of cirrus cloud formation: Homogeneous freezing of supercooled aerosols, *J. Geophys. Res.*, *107*(D2), 4010, doi:10.1029/2001JD000470.

Kärcher, B., A. Dörnbrack, and I. Sölch (2014), Supersaturation variability and cirrus ice crystal size distributions, *J. Atmos. Sci.*, *71*, 2905–2926, doi:10.1175/JAS-D-13-0404.1.

Kienast-Sjögren, E., A. K. Miltenberger, B. P. Luo, and T. Peter (2015), Sensitivities of Lagrangian modeling of mid-latitude cirrus clouds to trajectory data quality, *Atmos. Chem. Phys. Discuss.*, *15*(5), 7535–7584, doi:10.5194/acpd-15-7535-2015.

Kim, J.-E., and M. J. Alexander (2015), Direct impacts of waves on tropical cold point tropopause temperature, *Geophys. Res. Lett.*, *42*, 1584–1592, doi:10.1002/2014GL062737.

Massman, W. J. (1978), On the nature of vertical oscillations of constant volume balloons, *J. Appl. Meteorol.*, *17*, 1351–1356, doi:10.1175/1520-0450(1978)017<1351:OTNOVO>2.0.CO;2.

Muhlbauer, A., H. Kalesse, and P. Kollias (2014), Vertical velocities and turbulence in midlatitude anvil cirrus: A comparison between in situ aircraft measurements and ground-based doppler cloud radar retrievals, *Geophys. Res. Lett.*, *41*, 7814–7821, doi:10.1002/2014GL062279.

Murphy, D. M. (2003), Dehydration in cold clouds is enhanced by a transition from cubic to hexagonal ice, *Geophys. Res. Lett.*, *30*(23), 2230, doi:10.1029/2003GL018566.

Murphy, D. M. (2014), Rare temperature histories and cirrus ice number density in a parcel and a one-dimensional model, *Atmos. Chem. Phys.*, *14*(23), 13,013–13,022, doi:10.5194/acp-14-13013-2014.

Murphy, D. M., and B. L. Gary (1995), Mesoscale temperature fluctuations and polar stratospheric clouds, *J. Atmos. Sci.*, *52*(10), 1753–1760, doi:10.1175/1520-0469.

Nastrom, G. D. (1980), The response of superpressure balloons to gravity waves, *J. Appl. Meteorol.*, *19*, 1013–1019, doi:10.1175/1520-0450(1980)019<1013:TROSBT>2.0.CO;2.

Oppenheim, A. V., R. W. Schafer, and J. R. Buck (1999), *Discrete-Time Signal Processing*, 1st ed., Prentice-Hall, Upper Saddle River, N. J.

Podglajen, A., A. Hertzog, R. Plougonven, and N. Žagar (2014), Assessment of the accuracy of (re)analyses in the equatorial lower stratosphere, *J. Geophys. Res. Atmos.*, *119*, 11,166–11,188, doi:10.1002/2014JD021849.

Rabier, F., et al. (2010), The Concordiasi project in Antarctica, *Bull. Am. Meteorol. Soc.*, *91*, 69–86, doi:10.1175/2009bams2764.1.

Randel, W. J., and E. J. Jensen (2013), Physical processes in the tropical tropopause layer and their roles in a changing climate, *Nat. Geosci.*, *6*(3), 169–176, doi:10.1038/ngeo1733.

Solomon, S., R. R. Garcia, S. F. Rowland, and D. J. Wuebbles (1986), On the depletion of Antarctic ozone, *Nature*, *321*, 755–758, doi:10.1038/321755a0.

Solomon, S., K. H. Rosenlof, R. W. Portmann, J. S. Daniel, S. M. Davis, T. J. Sanford, and G.-K. Plattner (2010), Contributions of stratospheric water vapor to decadal changes in the rate of global warming, *Science*, *327*(5970), 1219–1223, doi:10.1126/science.1182488.

Spichtinger, P., and M. Krämer (2013), Tropical tropopause ice clouds: A dynamic approach to the mystery of low crystal numbers, *Atmos. Chem. Phys.*, *13*(19), 9801–9818, doi:10.5194/acp-13-9801-2013.

Tabazadeh, A., O. B. Toon, B. L. Gary, J. T. Bacmeister, and M. R. Schoeberl (1996), Observational constraints on the formation of type Ia polar stratospheric clouds, *Geophys. Res. Lett.*, *23*(16), 2109–2112, doi:10.1029/96GL01998.

Vial, F., A. Hertzog, C. R. Mechoso, C. Basdevant, P. Cocquerez, V. Dubourg, and F. Nouel (2001), A study of the dynamics of the equatorial lower stratosphere by use of ultra-long-duration balloons: 1. Planetary scales, *J. Geophys. Res.*, *106*(D19), 22,725–22,743, doi:10.1029/2000JD000241.

Vincent, R. A., and S. D. Eckermann (1990), VHF radar observations of mesoscale motions in the troposphere: Evidence for gravity wave Doppler shifting, *Radio Sci.*, *25*(5), 1019–1037, doi:10.1029/RS025i005p01019.

Vincent, R. A., and A. Hertzog (2014), The response of superpressure balloons to gravity wave motions, *Atmos. Meas. Tech.*, *7*, 1043–1055, doi:10.5194/amt-7-1043-2014.

Voigt, A., and T. A. Shaw (2015), Circulation response to warming shaped by radiative changes of clouds and water vapour, *Nat. Geosci.*, *8*, 102–106, doi:10.1038/ngeo2345.